A Mesoscale-Microscale approach for the energy analysis of buildings

IOP Conf. Series: Journal of Physics: Conf. Series **1224** (2019) 012022 doi:10.1088/1742-6596/1224/1/012022

A Mesoscale-Microscale approach for the energy analysis of buildings

S Montelpare[1], V D'Alessandro[2], C Lops[1], E Costanzo[2] and R Ricci[2]

[1] University "G. d'Annunzio" of Chieti-Pescara, Engineering and Geology Department (INGEO)
Viale Pindaro 42, 65127 Pescara (Italy)
[2] Marche Polytechnic University, Industrial Engineering and Mathematical Sciences Department (DIISM)
Via Brecce Bianche 1, 60131 Ancona (Italy)

E-mail: s.montelpare@unich.it

Abstract. This work is aimed to suggest a numerical approach able to select the most useful building orientation with respect to the local wind in complex urban areas. It is showed a mesoscale-microscale numerical approach able to predict local flow patterns for building designers. The city of Ancona was selected to analyse wind patterns over complex orography in presence of buildings. The analysed area is characterized by a densely built hilly promontory flanked by a poorly urbanized valley. Two buildings were chosen to carry out energy analyses. At first, the MM5 weather prediction model is used to assess the wind patterns and the wind occurrence distribution. The 2010 year was simulated and compared with real data from a met-mast. After, computational fluid dynamic (CFD) analyses are conducted with and without the surrounding buildings to appreciate speed and inflow effects. CFD results showed great changes in the examined building area. The final step was the energy simulation, by means of EnergyPlus, of two multistoried buildings equipped with a double skin façade; results show a great impact on the energy consumption by comparing a wrong orientation with respect to the best solution derived from the mesoscale-microscale approach.

1. Introduction

Nowadays, "sustainable" is the new keyword of progress and the low environmental impact of buildings is a must. The basic principles of sustainable design integrate the traditional criteria of functionality, cost containment and aesthetic results, with environmental factors, health and well-being of building occupants. In this background, surveys aimed at defining the typical characteristics of the climate in a building site and the study of the interaction between the wind resources and the urban landscape assumed an increasing interest. Geographic position, terrain orography, meteorological parameters, play an important role for the wind resource of a site, but a direct survey is not always feasible. More and more frequently, the techniques to obtain this information involve a numerical approach and the use of scale models in wind tunnel; in both this techniques there is a common fundamental data, how to recreate the ABL and the ASL. Toparlar et al. [1] provides a review of research reported in journal publications on this topic till the end of 2015, by categorizing them on the morphology of the urban area (generic versus real) and on the methodology (with or without a validation procedure). They observe that CFD studies for generic urban areas typically involve simple building shapes, such as cubes

or rectangular prisms, and do not consider validation; when present, this is normally carried out with data from wind-tunnel measurements. CFD studies on real urban areas are normally realized without validation and they are comparative studies of several urban configurations and design parameters; almost all these studies are conducted with steady Reynolds Averaged Navier-Stokes (RANS) approaches. Blocken [2] reviews the importance of urban physics related to the societal challenges and provides some views on CFD: possibilities and limitations are discussed, and tips and tricks for accurate and reliable CFD simulations are illustrated. He underlines that the flow in an atmospheric boundary layer (ABL) is inherently unsteady and therefore, excluding (LES) because of the high computational efforts, an unsteady RANS approach should be required to resolve the unsteady mean-flow structures, while modelling the turbulence. Several studies [3, 4] analyse the impact of computational parameters on the numerical outcome for wind flow pattern. Other studies [5] analyse the coupling of mesoscale meteorological models (MMM) with computational wind engineering (CWE) models to produce realistic simulations; they focus the attention on up-scaling or downscaling methodologies [6] and on the effects related to energy buildings issues [7, 8, 9, 10, 11, 12, 13]. Some authors have focused their attention to the convective heat transfer coefficients in urban neighborhoods [14, 15, 16, 17], others on the air temperature in complex urban areas [18, 19] or on the Urban Heat Island (UHI) [20, 21].

This paper is aimed to evaluate the feasibility and the results of a holistic approach, based on a meso/micro scale numerical approach, which starts from a meteorological hindcast and finishes in a building energy simulation (BES) analysis by employing a CFD instrument to connect the different geometric scales. First of all, the paper checks the validity of the meteorological hindcasting simulation, then evaluate the effect of the local urbanization and finally quantifies the energy demand differences between a generic orientation and an orientation optimized by the proposed approach. In particular, the paper is divided into the following sections. Section 2 describes the case study. Section 3 illustrates the mesoscale approach, the adopted model explaining the settings and presenting the results obtained. Section 4 describes the microscale CFD approach, the computational domain, the numerical model and its outputs. Section 5 illustrates the energy analysis approach and the corresponding results. Finally, Section 6 summarizes the main achievements of the paper.

2. The Case Study

The methodology proposed in this paper is applied to a couple of buildings located in the city of Ancona and precisely in an urban expansion area characterized by a densely built hilly promontory flanked by a poorly urbanized valley (Fig.1). Both Buildings present a multy storey (Fig.2) double skin facade (DSF) whose performance is deeply influenced by the wind speed and direction and, for this reason, they are particularly suitable for the present work.

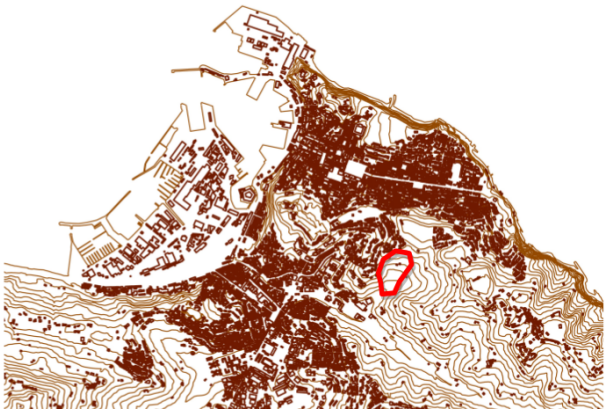

Figure 1: The analyzed area.

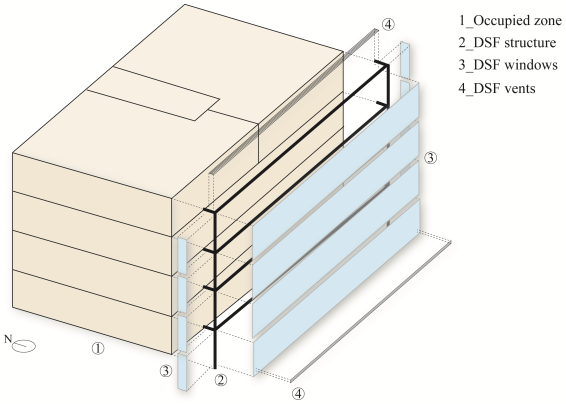

Figure 2: Simulated building.

3. The Mesoscale Approach

A mesoscale analysis was carried out in order to describe the climatology of the area of interest and in particular the wind assessment. A hindcasting procedure over a complete year (01/01/2010 - 31/12/2010) was performed adopting the version of a largely used meteorological code, properly modified by our research group.

3.1. The Meteorological Model

MM5v3, the PSU/NCAR Mesoscale Model Fifth Generation (MM5), is *a limited-area, nonhydrostatic, terrain-following sigma-coordinate model designed to simulate or predict mesoscale atmospheric circulation.* The MM5v3 official version is able to ingest digital terrain models and terrain land uses with a resolution of 30sec; the version used in this paper is a modified in order to be able to work also with the NASA Shuttle Radar Topography Mission (SRTM) 3sec Digital Terrain Elevation Model (DTEM) and with the high definition Corine European Land Cover database. These new skills were developed by our research group by modifying the FORTRAN code of the TERRAIN module; in this way it is possible to carry out simulations with a horizontal grid spacing down to 200 [m], describing with more accuracy complex orographies like the area of *Monte Conero* in Ancona (the object of this work).

3.2. The Numerical Set-up

The adopted operative procedure involves the use of a 2-way nesting approach with 5 domains, having the same center (longitude 13.519827°E, latitude 43.605847°N) and the same number of grid points (961), but with an increasing grid spacing; in particular, a growth ratio of 3 and an Arakawa-Lamb B-staggering (Fig.3b). Each domain extends in the vertical direction by 27 pressure sigma levels (Fig.3a), starting from 10 $[m]$ up to 10532 $[m]$ above surface level. Details about the domain settings are reported in Table 1:

Table 1: Domain settings table.

Name	Grid Spacing	Grid Points	Domain Extension
Domain 1	0.2 [km]	31x31	6x6 $[km^2]$
Domain 2	0.6 [km]	31x31	18x18 $[km^2]$
Domain 3	1.8 [km]	31x31	54x54 $[km^2]$
Domain 4	5.4 [km]	31x31	162x162 $[km^2]$
Domain 5	16.2 [km]	31x31	486x486 $[km^2]$

The use of a relatively high number of nested domain allows to take into account meteorological phenomena ranging from the synoptic scale down to the local one. The domain 1 (Fig.5) covers a large part of the Italian topography and also the Adriatic basin with the Croatian coasts; at this synoptic scale it is possible to evaluate the main perturbation phenomena that occur with weekly or monthly frequency (Fig.4). Domain 5 (Fig.6) covers, instead, the region nearby the area of interest and describes the terrain slopes with more accuracy; in this way it is possible to better describe local convective phenomena like sea or hill breezes that occur with 12h or 24h frequencies.

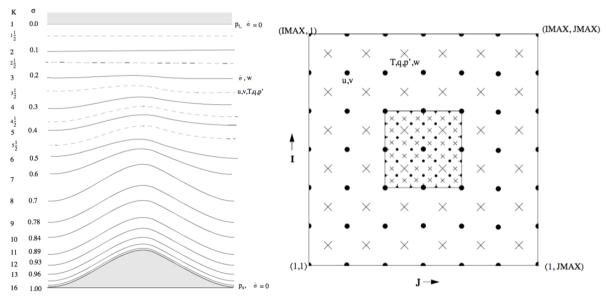

Figure 3: MM5 Pressure Sigma Levels (a) and Arakawa B Nesting Schema (b).

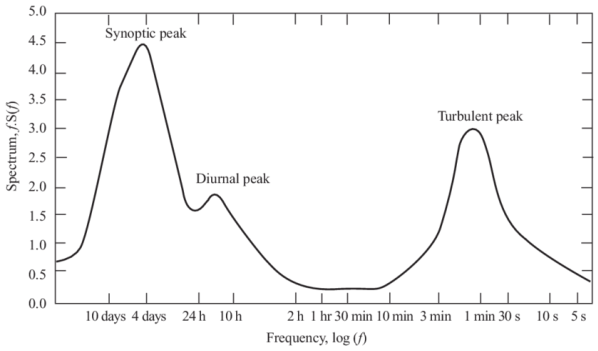

Figure 4: Wind Spectrum Farm Brookhaven based on work by Van der Hoven (1957).

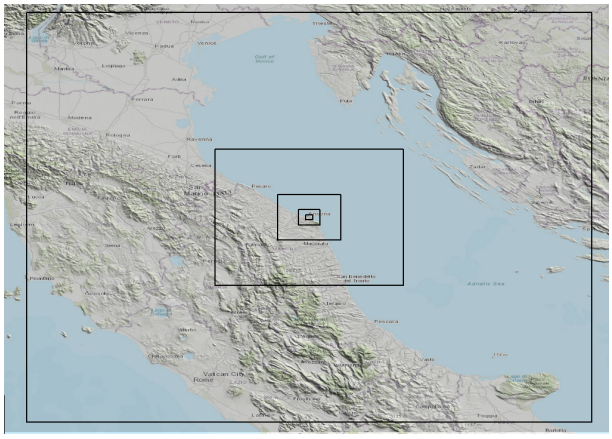

Figure 5: Domain nesting.

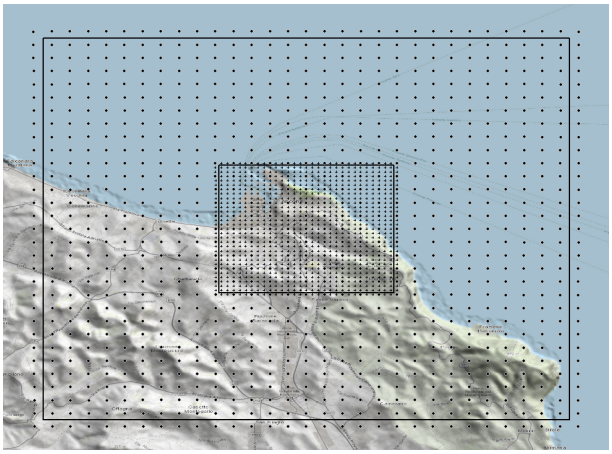

Figure 6: Domain 4 vs Domain 5.

The adopted meteorological input is the NCEP ds083.2 datasets, belonging to the FNL Operational Model Global Tropospheric Analyses; these data are available on 1-degree by 1-degree grids with a 6hs-time interval and they are from the Global Data Assimilation System (GDAS), which continuously collects observational data from the Global Telecommunications System (GTS) and other sources (as meteorological stations, met-balloons, met-tower, ships etc..) from all around the world. These inputs are interpolated on the 31x31 outer domain horizontal grid by the REGRID module and on 27 pressure full sigma levels by the INTERPF module. Finally, the MM5 module resolves a complete set of equations (pressure, momentum, thermodynamics, moisture etc.) to output a four dimensional database of climatic variables (air

pressure, air and soil temperature, wind speed and direction, humidity, radiation etc.) with a 4 mins-time step and a 200 $[m]$ horizontal resolution.

The physics options adopted to solve the simulation domains are:

Table 2: MM5 Physics Options.

Physics Option	Domain 1	Domain 2	Domain 3	Domain 4	Domain 5
$IMPHYS_{\_MoistureScheme}$	Simple Ice	Simple Ice	Simple Ice	Simple Ice	Simple Ice
$ICUPA_{\_CumulusScheme}$	KF2	KF2	None	None	None
$IBLTYP_{\_PlanetBound.Layer}$	MRF	MRF	MRF	MRF	MRF
$FRAD_{\_Atm.Radiation}$	RRTM	RRTM	RRTM	RRTM	RRTM
$ISOIL_{\_SoilTemp.Model}$	Noah LSM	Noah LSM	Noah LSM	Noah LSM	Noah LSM

The MM5 outputs are post-processed to obtain wind and solar maps, windroses and time histories of the main climatic parameters: i.e. planet boundary layer height, vapour mixing ratio, wind speed components, wind direction, ground temperature, air temperature, surface downward shortwave radiation, surface downward longwave radiation, pressure, humidity.

Time histories are rearranged in form of virtual meteorological masts having a measurement plane for every sigma level; for the purpose of the present research, only the lowest 8 heights were extracted, corresponding to $10, 30, 51, 71, 92, 122, 163, 204, 255, 321, 407$ and $509[m]$.

3.3. The Mesoscale Results

Figures 8 and 7 report some windroses extracted at the same positions but different heights above the surface layer: i.e. $10[m]$ and $509[m]$. Observing the figure 8 it is possible to note that the wind intensities distribution is the same while the occurrences are slightly different only for the western sectors. Figure 7 shows, instead, marked differences both in terms of speed intensities and prevalent directions: the points over the sea have lower velocities, as expected for their lower height, but the same behaviour, while others located around the city exhibit stronger velocity decrease and also marked inflows due to the terrain conformation and the land use. The presence of a steep hills in the southern part of the city influences the wind distribution by aligning the flow along the main axis.

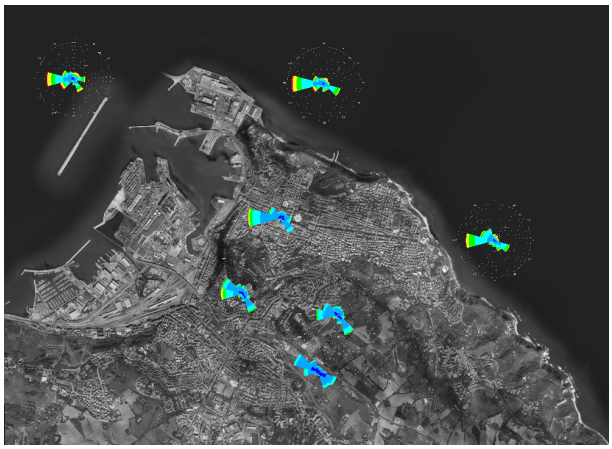

Figure 7: Annual wind roses @ 10[m] asl.

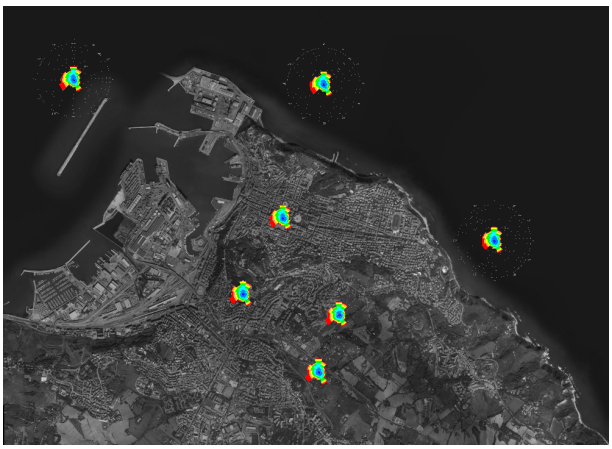

Figure 8: Annual wind roses @ 509[m] asl.

These results corroborate the paper initial hypothesis that a meso-micro approach could better support the energy analysis in complex terrain. In fact, the use of the equation 1 in

BESs, as suggested by Ashrae 2001, can not completely describe the local modification of the meteorological mast. This equation converts the meteorological wind speed from the EnergyPlus Weather (EPW) file to the local wind speed by using the α and δ values in correspondence of the meteorological station and building location. These values, reported in table 3, take into account the effects that the land use induces on the height of an atmospheric surface layer and on the wind speed profile, but they do not consider orographic speed-up and inflow effects.

$$U_{loc} = U_{met}\left(\frac{\delta_{met}}{z_{met}}\right)^{\alpha_{met}}\left(\frac{z}{\delta}\right)^{\alpha} \tag{1}$$

Table 3: Terrain dependent coefficients (ASHRAE 2001).

Terrain	Description	Exponent α	Layer Thickness $\delta[m]$
1	Flat, open country	0.14	270
2	Rough, wooded country	0.22	370
3	Towns and cities	0.33	460
4	Ocean	0.10	210
5	Urban, industrial, forest	0.22	370

The equation 1 derives from equation 2 considering 2 different assumptions: the gradient wind, the wind speed at the atmospheric boundary layer (ABL) top, is the same over the meteorological station and over the local building, the boundary layer height assumes the values reported in the table 3 without transition mixing zones. The former assumption is quite acceptable while the latter is more difficult to satisfy in case of different land uses in relatively small areas.

$$U_1 = U_2 \cdot \left(\frac{z_2}{z_1}\right)^{\alpha} \tag{2}$$

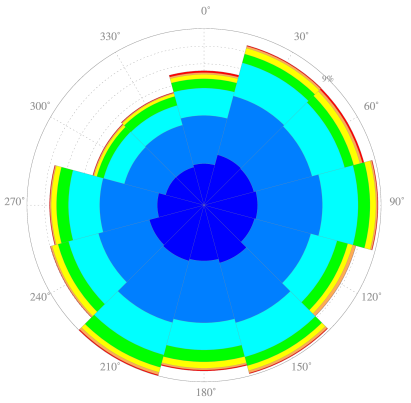

Figure 9: EnergyPlus Ancona EPW windrose

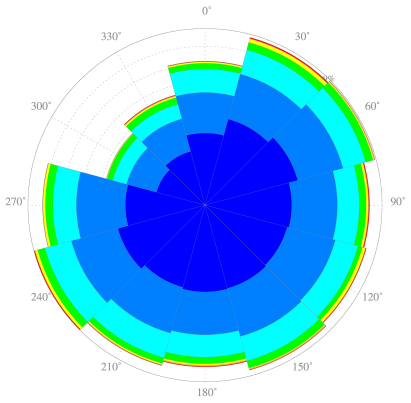

Figure 10: EnergyPlus Ancona-Falconara EPW windrose

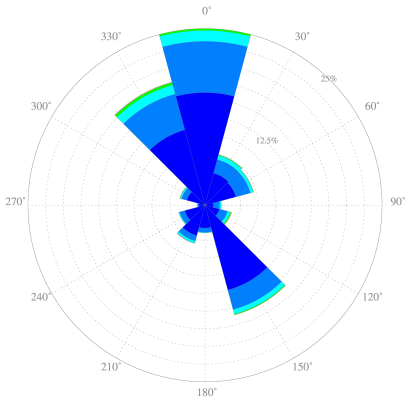

Figure 11: SIRMIP Ancona 2010 windrose

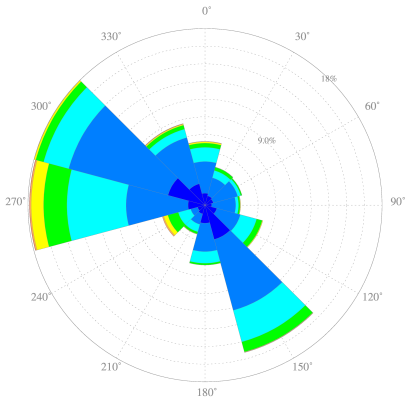

Figure 12: microMM5 Ancona 2010 windrose

Figures 9-12 show the annual windroses for: the available EnergyPlus Weather files (i.e. Ancona and Ancona-Falconara), the SIRMIP meteorological mast (installed on the roof of the building of Marche Region) and a microMM5 virtual mast extracted in the same coordinates of the real one. The SIRMIP met-mast is the closest to the area of study. Both the EnergyPlus windroses show very similar directional occurrences but exhibit different wind speeds: globally it is possible to note a large spread of direction occurrences. Contrarily, the SIRMIP met-mast and the microMM5 virtual mast exhibit more defined directions and show a different rotation of 60° only for the northern occurrences: this difference could be related to the SIRMIP positioning, because it is installed on the top of a large and tall building that locally modifies the flow pattern and the microMM5 code is not able to describe this local phenomenon. However, it is possible to say that in general the mesoscale approach is able to better describe the annual measurements of the closest real anemometer.

4. The CFD Approach

CFD analysis was carried out on a large computational domain to include the speed-up and inflow effects generated by the nearby complex orography. In addition, the presence of buildings in the surrounding districts was evaluated in order to estimate their influence on the observed area.

4.1. The Computational Domain

The first step of the microscale approach was the realization of the computational domain and the choice of the mesh sizes. The primary aspect to be considered is the digital terrain model because the coastal area of Ancona is characterized by high cliffs and the only use of a detailed cartography (1:200 CTR Charts) can correctly reproduce this complexity. A custom Matlab procedure was developed to extract the intersection points among each contour line and the radial lines starting from the domain center and spanning all the circumference at every 2°; in this way, a cloud of about 110k points was obtained to generate the mesh. Figure 13 reports these points from isocontour at $10[m]$ and the high density of points of the coastline is clearly visible. The cloud of points was then shifted to have the lower elevation corresponding to a $0[m]$ value and, subsequently, a smoothing procedure, using a bell function, was performed to obtain a flat terrain all around the external part of the simulation domain (Fig.14); these changes have been made to avoid discontinuity in the incoming inlet wind velocity profile. The obtained computational domain is a cylindrical volume having a circular plant with a radius of 6 $[km]$; it is subdivided into three concentric annular zones centered on the building position analysed [2]. The outer annulus, deformed by the bell function, is considered as smooth, the central one is

described with an equivalent roughness, corresponding to the local land use, and the inner circle takes in account the real buildings. The height of the cylinder ($750[m]$) was selected in order to have a blockage ratio lower than or equal to 3% for the most disadvantaged section [2, 22]; i.e. the cross plane having the highest terrain profile. The cylinder external surface was subdivided into 12 sectors to describe all the wind directions reported in the windroses previously showed. Considering that the aim of this paper was to evaluate the proposed multiscale computational approach, the only results referred to the western winds are here reported.

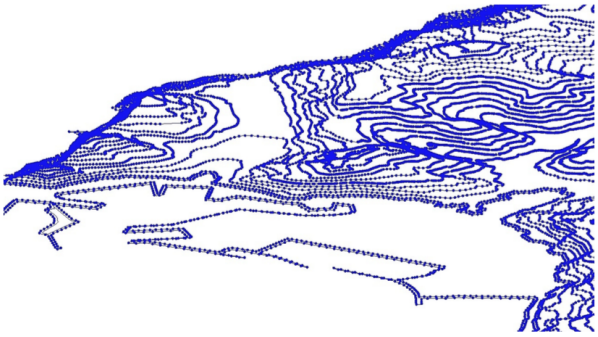

Figure 13: Isocontour Ancona.

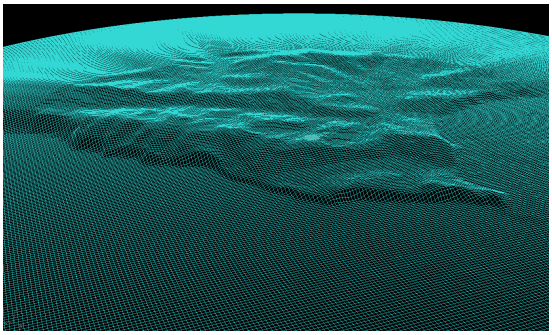

Figure 14: CFD terrain mesh.

Two grids were created: the former, with only the test case buildings, uses a refinement volume around the area of interest and has 2118000 cells (Fig.15). The latter, with all the other buildings present in the surrounding districts, has 1458811 cells and involves the use of two different roughness length to change the height of the first cell at wall (Fig.16). This double model was used to evaluate the flow perturbations caused by the existing surrounding built.

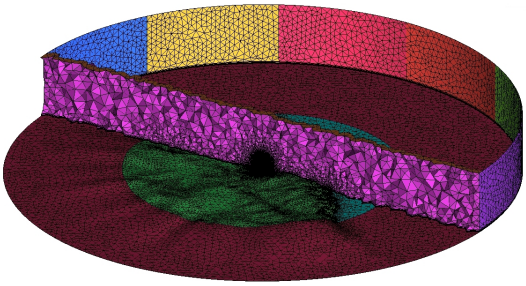

Figure 15: CFD computational domain.

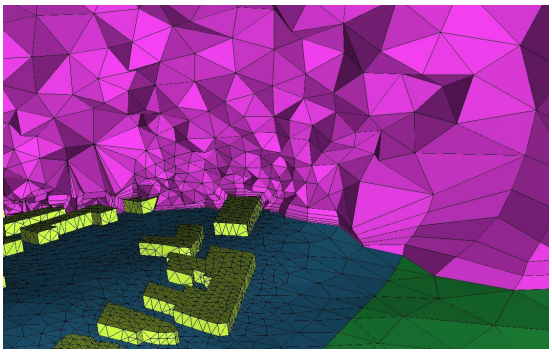

Figure 16: Mesh detail around buildings.

4.2. The Boundary Conditions

The inlet boundary condition was set as an atmospheric flow, following the exponential wind profile described in the equation 2 with an α value of 0.2. This condition, by fixing the $x-y$ direction of the incoming wind, was applied for 6 sectors of the cylinder external surface, while in the other 6 a pressure inlet outlet condition was settled. The domain upper surface was defined with a no-slip condition, while the base of the outer annulus was settled with a slip condition on the smooth surface. The intermediate annulus and the central area were settled as rough surfaces. The numerical model does not use the aerodynamic roughness z_0 typically implemented in the von Karman law (eq.3) but the equivalent Nikuradse roughness K_s. The wall law used in the numerical model is reported in equation 4 where the E value is about 9 and the ΔB value is a constant depending on the dimensionless equivalent roughness K_s^+ (eq.5). The

ΔB value represents a vertical translation of the logarithmic wind profile due to the presence of the roughness. In the present study, a fully rough regime having K_s^+ greater than 90 could be assumed; with the present assumption, the Nikuradse equivalent roughness could be evaluated with the equation 6, where the constant $C_s = 0.5$ and $E \approx 9$.

$$U(z) = \frac{u^*}{k} \cdot \ln\left(\frac{z}{z_0}\right) \tag{3}$$

$$u_p = \frac{u^*}{k} \ln\left(E\frac{\rho u^* z_p}{\mu}\right) - \Delta B \tag{4}$$

$$K_s^+ = \frac{\rho K_s u^*}{\mu} \tag{5}$$

$$K_s = \frac{z_0 E}{C_s} \tag{6}$$

Finally, the values of the Nikuradse equivalent roughness assumed for the computational domain are reported in table 4:

Table 4: Domain settings table.

Domain Surface	K_s
Sea	0.19586
Test area terrain	0.2
Intermediate annulus terrain	3.52

The least boundary condition is referred to the building surfaces, that are considered smooth and with a slip condition.

4.3. The Numerical Model

Unsteady simulations were carried out by using a Reynolds Stress (RSM) turbulence model; preliminary analyses on 2D (Almeida Hill) and 3D (Askervein Hill) test cases showed that two equation models like $k-\epsilon$ and $k-\omega$ are not able to accurately describe flow separations. The seven equation Reynolds Stress Model has instead demonstrated to be able to simulate complex flows by using transport equations for the six independent Reynolds stresses in addition to the equation for the turbulent dissipation; the counterpart is a higher computational effort.

4.4. The CFD Results

CFD simulations showed a significant effect of the nearby buildings on the wind speed distribution in the proximity of the test buildings and also a great effect on the wind directions with marked deviations of the inflow angle. Figure 17 shows the points where a vertical profile of the mentioned variables were extracted. Results are presented both in terms of vertical profiles and as visual maps.

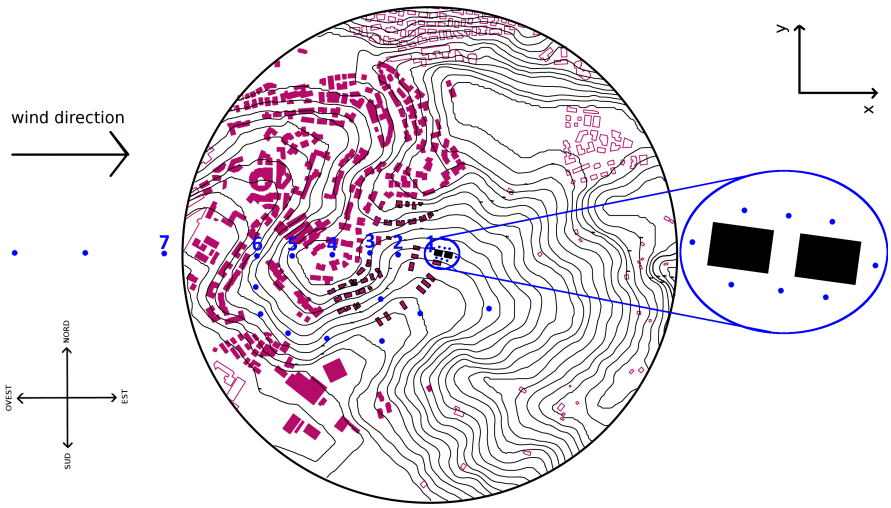

Figure 17: CFD extraction points.

As figures 18 and 19 show, the local terrain conformation and the presence of nearby buildings, even if at distance greater than 100$[m]$, are able to strongly influence the wind speed distribution up to about 80$[m]$ above the surface layer. It should be considered that the buildings located inside the area of study are typically three or five stories and with height below 15$[m]$.

By observing the figure 17 it is possible to note that the point corresponding to the terrain maximum height is the number 4 and that the western wind encounters the test building downstream a hill, in a zone of pressure recovery.

The absence of nearby buildings better explains the effects directly related to the terrain local conformation: it is possible to see a marked speed-up from the point 7 up to the top of the hill (points 4 and 3), while the pressure recovery downstream the summit justifies the velocity decrease. The graph of the wind inflow deviation shows a significant deviation for the points upstream the hill, while the points near the area of study do not exhibit meaningful flow deflections. Globally, it is possible to say that the orographic effects induce, in the test buildings area and for western wind, appreciable effects on the wind speed but not on the direction.

Figure 19 shows very different behaviour with respect to the previous case: excluding the point 7, that is the region where buildings are simulated as an equivalent roughness, and the point 5, that is in an area with few buildings, all the other points exhibit irregular wind profiles with points 1 and 6 that have a constant velocity for the lower height, underlying the presence of flow separation areas. The point just upstream the test buildings (point 1) presents a velocity decrease, at a height of 12$[m]$, of about 50%. The graph of the inflow deviation shows also great effects due to the presence of nearby buildings. The point 6 and the test building point (n^o1) have very opposite behaviour with angles of deviation up to 25° both positive and negative. Globally, it is possible to say that the presence of nearby buildings is a main parameter to take into account for evaluating the incoming wind speed profile to a specific area of interest: both the wind velocity and direction are strongly modified.

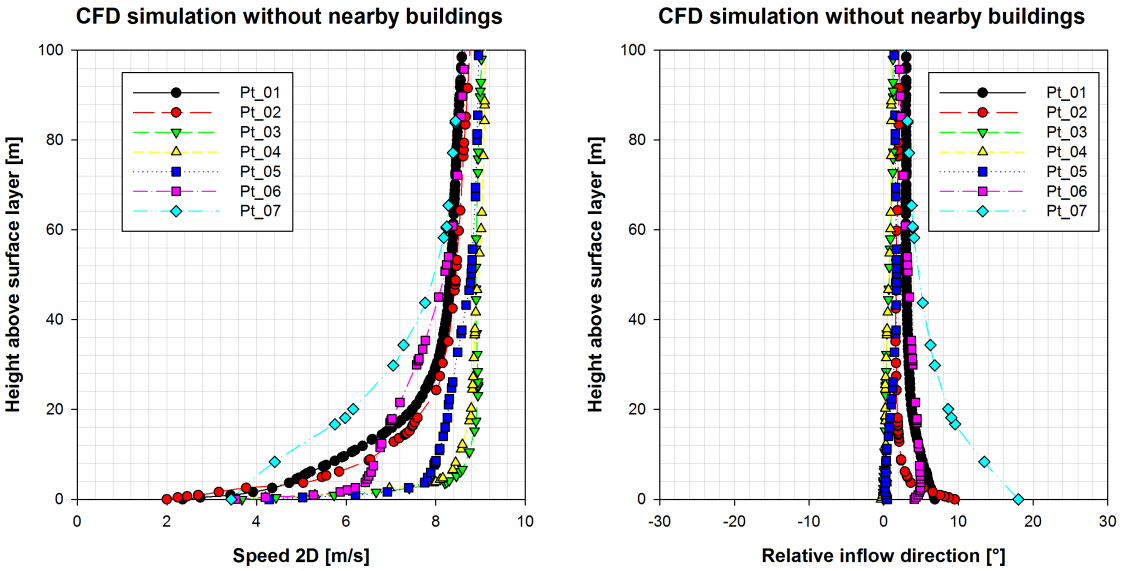

Figure 18: Wind Speed and Inflow deviation without nearby buildings.

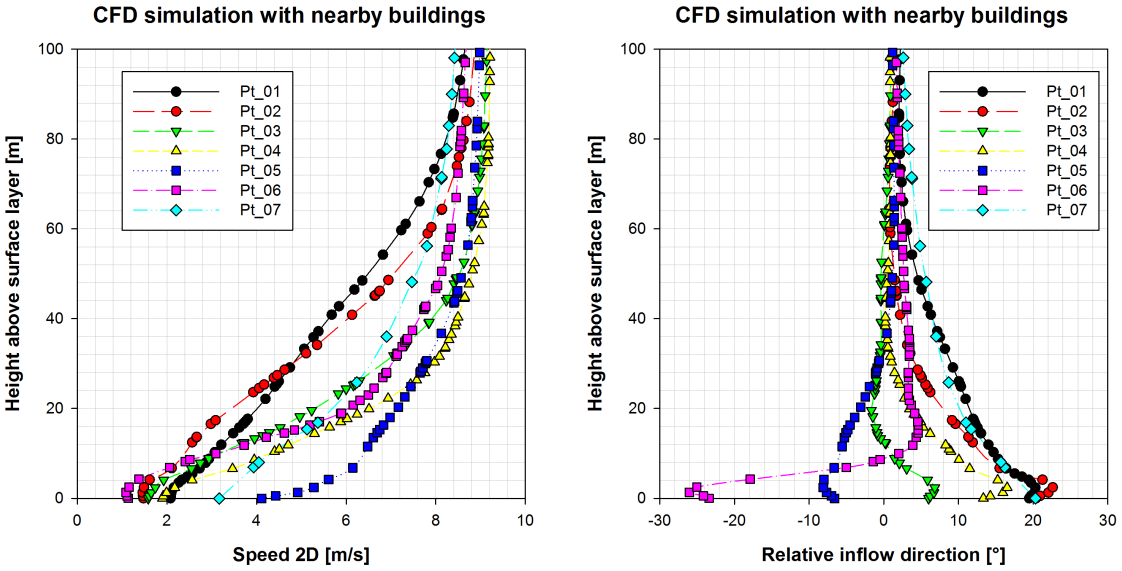

Figure 19: Wind Speed and Inflow deviation with nearby buildings.

5. The Building Energy Analysis

Dynamic energetic simulations have been carried out in order to estimate the reduction in terms of building cooling requirement and define the variation of the DSF performance, considering the main wind directions.

5.1. The Model Set-up
The case study is a residential building, dating from the second Italian postwar, and made of reinforced concrete. It has a rectangular shape with sizes equal to 22 x 11.5 metres, with four levels above ground for a total high of 12.2 metres. Its main axis direction is perfectly towards the East-West directrix. Table 5 summarizes the transmittance (K) values of the building envelope.

Table 5: K values for building components.

Element	$s[m]$	$K[\frac{W}{m^2K}]$
External wall	0.30	1.13
Floor	0.08	3.00
Roof	0.25	1.40
Partition	0.15	1.60
Window	0.01	3.16

On the South elevation, a naturally ventilated and multi storey double skin façade is present. It means that the cavity between the inner and the outer layers of the DSF has inlet and outlet vents that allow the natural ventilation inside the enclosed space. The cavity is 1 $[m]$ depth and extends over the total height of the building, without any separation. The external skin is made of single glazed windows with K value equal to 5.80 and, in order to avoid the overheating of the air volume in the cavity, it has an integrated shading system composed of external blinds with medium reflectivity slats and solar control type fixed at $120[W \cdot m^{-2}]$. The inlet and the outlet vents are located respectively on the bottom and the top of the double skin façade. Internal grills are placed on the inner layer of the DSF, ensuring an adequate ventilation of the occupied zone. These grills, both the internal and external ones, allow continually the air to enter the cavity and the whole building during the hottest period and they are closed in the winter time when the cavity becomes sealed and its ventilation is not allowed in order to decrease the transmittance of the façade and reduce the heat losses. The infiltration rate of the building is $0.7[m^3 \cdot s^{-1}]$ and the control mode for the calculated natural ventilation, both for the cavity and the building, is constant. This means that whenever an opening's operation schedule allows venting, all of the zone's openable windows and doors are open. The air temperature distribution model for each zone is mixed and it is considered uniform through the zone. The DSF cavity, at the zone level, is set as unoccupied by loading, heating/cooling and lighting template data. The plant system of the building involves the presence of natural gas boilers with an efficiency around 85%, for the heating need, and split system with a coefficient of performance equal to 1.8 for the summer period. The case study has been analysed through dynamic analysis in Energy Plus, considering as simulation period the typical summer week (19 – 25 August) that is identified by the weather data translator as being typical of the summer.

5.2. The Building Energy Simulation Results
The building energy simulations are performed in Energy Plus, using its graphical interface DesignBuilder. Table 6 and Figures 20 and 21 show respectively the impact that different wind directions have on the performance of a building with a double skin façade in terms of cooling requirement and air flow rate in the DSF cavity. The simulations consider as main wind directions two cases: the first case analyses the possibility of a wind which impacts directly on the DSF, coming from the South (180°), and the second one studies the opposite condition, with a Northern wind (0°). According to the energetic simulations, the Southern wind, impacting directly on the DSF, can reduce the building cooling requirement of the 10% as it is shown in Table 6.

Table 6: Building cooling requirement with different wind directions.

Wind direction	Cooling requirement $[kWh[$
South Wind	605
North Wind	662

In addition, the air flux that enters and goes out from the vents, located respectively at the bottom and the top of the cavity of the double skin façade, is higher with a 180°wind direction and the difference between the two configurations reaches $2[m^3 \cdot s^{-1}]$ during specific daily hours.

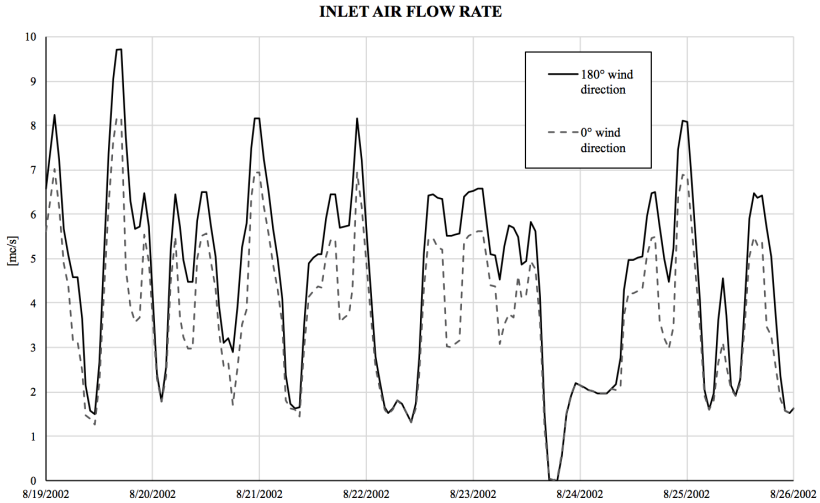

Figure 20: Inlet air flow rate.

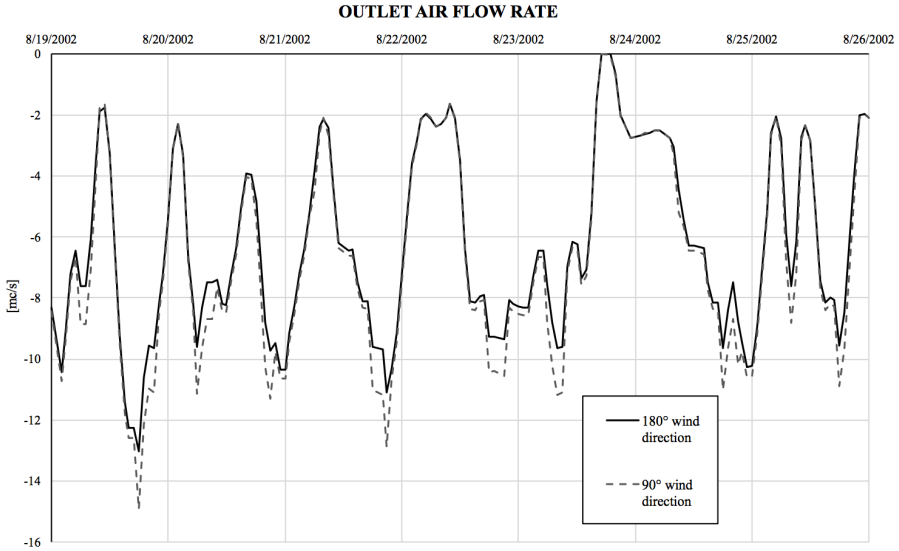

Figure 21: Outlet air flow rate.

The dynamic energy simulations highlight how the most efficient condition for a building with a double skin façade is reached when the wind impacts directly on the grills of the DSF cavity, ensuring the highest amount of natural ventilation, both in the cavity and in the whole building, and involving a consequent reduction in terms of energy consumption for the cooling need of the occupied zones. For a more accurate estimation of the natural ventilation inside the DSF cavity related to different wind directions, a coupling approach between energy simulation and computational fluid dynamic analysis should be adopted. As suggested in [23] and [24], in fact, the energy simulation programs assume that the air in an indoor space is uniform and the convective heat transfer coefficients available for the analyses are usually empirical and not accurate. Therefore, coupling the energy simulation with the CFD analysis is a good option to overcome these limits in order to obtain more realistic and reliable results.

6. Conclusions

This paper was aimed to evaluate the feasibility and the results of a holistic approach able to improve the energy analysis of buildings in complex urban environments. The city of Ancona was selected as the area of study because it shows the combination of a complex orography with high density urban areas; in particular, two buildings, equipped with a double skin façade, were identified as the object of the energy analyses. The first step of the proposed approach is a hindcasting meteorological analysis by means of the MM5v3 NWP model; this code was modified to ingest a high definition digital terrain model (the SRTM 3s DTM) and also a high resolution land use database (the European CORINE). A nesting procedure, with five domains, allowed to obtain information from synoptic scales down to local ones. Results show a strong influence of the local orography with marked differences among the extracted numerical windroses. The comparison between the MM5 virtual meteorological mast and the real one installed on the top of the “Marche Region” building show a very good agreement underlining the reliability of the proposed hindcasting procedure for local climates. The second step was the simulation, with a CFD code, of the urban context nearby the analysed buildings. A computational domain with a blockage lesser than 3% was defined and it was divided into three concentric subdomains having different roughness descriptions: the inner is centred on the two analysed buildings and

considers also the nearby district buildings. The results of the CFD analysis allowed to obtain both the speed-up values and the inflow deviations of the wind approaching the test buildings. There are significant differences among the extracted points and between the simulations with and without the surrounding buildings: this underlines the necessity to correctly simulate the nearby urbanization in order to take into account local modification of the wind resource. The third step was an energy evaluation, by the DesignBuilder software, of the effects that a correct wind-building interaction may induce. A difference of about 10% on the cooling demand was obtained for the typical summer week, underlining the importance of a correct orientation and of a right local wind assessment. Synthetically the proposed procedure could be summarized in the subsequent step:

- A hindcasting simulation with a modified NWP code to obtain numerical met masts.
- A CFD simulation of the nearby urban area to estimate local speed-up and inflow values able to locally modify the numerical met mast.
- A BES analysis to evaluate the effect of natural ventilation on the cooling requirements.

Nomenclature

k	Von Karman constant
K_s^+	Dimensionless equivalent roughness
α	Wind power law exponent
μ	Dynamic viscosity $[\frac{m^2}{s}]$
ρ	Fluid density $[\frac{kg}{m^3 s}]$
K	Thermal transmittance $[\frac{W}{m^2 K}]$
K_s	Equivalent roughness $[m]$
U	Wind speed $[m/s]$
u^*	Friction velocity $[m/s]$
u_p	Wind speed at the center of the first wall cell $[m/s]$
z	Height above ground $[m]$
z_0	Roughness lenght $[m]$
z_p	Height of the center of the first wall cell $[m/s]$

References

[1] Toparlar Y, Blocken B, Maiheu B and van Heijst G 2017 *Renewable Sustainable Energy Rev.* **80** 1613–1640 ISSN 13640321
[2] Blocken B 2015 *Build. Environ.* **91** 219–245 ISSN 03601323
[3] Dhunny A, Samkhaniani N, Lollchund M and Rughooputh S 2018 *Urban Clim.* **24** 185–204 ISSN 22120955
[4] Liu S, Pan W, Zhang H, Cheng X, Long Z and Chen Q 2017 *Build. Environ.* **117** 11–23 ISSN 03601323
[5] Yamada T and Koike K 2011 *J. Wind Eng. Ind. Aerodyn.* **99** 199–216 ISSN 01676105
[6] Tewari M, Kusaka H, Chen F, Coirier W J, Kim S, Wyszogrodzki A A and Warner T T 2010 *Atmos. Res.* **96** 656–664 ISSN 01698095
[7] Srebric J, Heidarinejad M and Liu J 2015 *Build. Environ.* **91** 246–262 ISSN 03601323
[8] Allegrini J, Dorer V and Carmeliet J 2015 *Sustainable Cities and Society* **19** 385–394 ISSN 22106707
[9] Gracik S, Heidarinejad M, Liu J and Srebric J 2015 *Build. Environ.* **90** 15–29 ISSN 03601323
[10] Khoshdel Nikkho S, Heidarinejad M, Liu J and Srebric J 2017 *Appl. Therm. Eng.* **116** 850–865 ISSN 13594311
[11] Mauree D, Perera A and Scartezzini J L 2017 *Energy Procedia* **142** 2648–2654 ISSN 18766102
[12] Eleftheriadou A, Sfetsos A and Gounaris N 2016 *Energy Build.* **111** 176–183 ISSN 03787788
[13] Huang K T and Li Y J 2017 *Energy Build.* **154** 448–464 ISSN 03787788
[14] Liu J, Heidarinejad M, Gracik S and Srebric J 2015 *Energy Build.* **86** 449–463 ISSN 03787788
[15] Defraeye T, Blocken B and Carmeliet J 2011 *Energy Convers. Manage.* **52** 512–522 ISSN 01968904
[16] Montazeri H and Blocken B 2017 *Build. Environ.* **119** 153–168 ISSN 03601323
[17] Liu J, Srebric J and Yu N 2013 *Int. J. Heat Mass Transfer* **61** 209–225 ISSN 00179310
[18] Toparlar Y, Blocken B, Vos P, van Heijst G, Janssen W, van Hooff T, Montazeri H and Timmermans H 2015 *Build. Environ.* **83** 79–90 ISSN 03601323
[19] Allegrini J and Carmeliet J 2017 *Urban Clim.* **21** 278–305 ISSN 22120955
[20] Göndöcs J, Breuer H, Pongrácz R and Bartholy J 2017 *Urban Clim.* **21** 66–86 ISSN 22120955

[21] Allegrini J and Carmeliet J 2018 *Urban Clim.* **24** 340–359 ISSN 22120955
[22] Franke J, Hellsten A, Schlünzen H and Carissimo B 2007 *COST Action 732 - Best practice guideline for the cfd simulation of flows in the urban environment* ISBN 3-00-018312-4
[23] Zhai Z, Chen Q, Haves P and Klems J H 2002 *Build. Environ.* **37** 857–864
[24] Manz H and Frank T 2005 *Energy Build.* **37** 1114–1121 ISSN 03787788